
Article:
Dong, X., Griffo, A. orcid.org/0000-0001-5642-2921 and Wang, J. orcid.org/0000-0003-4870-3744 (2020) Multi-parameter model order reduction for thermal modelling of power electronics. IEEE Transactions on Power Electronics, 35 (8). pp. 8550-8558. ISSN 0885-8993

https://doi.org/10.1109/TPEL.2020.2965248

Multi-Parameter Model Order Reduction for Thermal Modelling of Power Electronics

Xiaojun Dong, Antonio Griffo, Jiabin Wang,
The University of Sheffield, Sheffield, UK

***Abstract*- In this paper, a multi-parameter model order reduction is applied to the thermal modelling and simulation of power electronics modules and air cooling system. Although widely employed, simulation tools based on Finite elements (FE) or finite difference methods (FDM) result in computationally expensive models that hamper the analysis in studies where one or more parameters are changed. Model order reduction techniques can be applied to reduce the computational complexity. However, standard reduction techniques cannot easily consider parameters variability and need to be reapplied for each parameter value. The paper proposes a multi-parameter order reduction technique which can significantly improve the thermal simulation efficiency without having a significant impact on the prediction accuracy. The method is applied to multi-chip SiC power module mounted on a forced air cooled finned heatsink with variable air flow.**

Index Terms— Thermal modelling; Power Electronics; Finite difference method (FDM); Multi-Parameter model order reduction (MOR); Air cooling.

I. Introduction

THE modeling of electro-thermal interactions for reliable design and management of power electronic systems is becoming increasingly important due to the growing demand for higher power density in energy conversion systems [1]. Reliability for power electronics has been an important issue since the early power electronic applications [2]. It is well known that the reliability of power electronic converters is significantly affected by operating temperature and thermal cycling as several ageing mechanisms and failure modes associated with devices and packaging are exponentially accelerated by temperature and temperature variations [3].

Consequently, the thermal management requirements for power converters design and operation are becoming more and more demanding [4]-[6]. Heat exchangers are often the largest contributors to volume and mass for power converters. Optimization of the thermal and heat dissipation design can therefore help increase the power density of the converter. Accurate thermal analysis modeling tools are, therefore, essential in the design optimization of power converters. Furthermore, compact thermal model can also be used to estimate and monitor component temperatures during real-time operation enabling the online health monitoring and prognostic of the converter [7].

Simple compact thermal models based on lumped parameter networks such as those based on Cauer or Foster networks are commonly used in power electronics design. Despite their computational efficiency, lumped parameter models (LPM) are of limited use at the design stage as they typically rely on empirical calibration, with values that cannot be directly correlated with design parameters such as topology of the layout, environmental and operating conditions. Cauer and Foster LPN are also typically one dimensional and do not account for the two-dimensional mutual thermal coupling between adjacent devices, although a 2D LPN has recently been proposed in [8]. Accurate physical representation of the converter topology and environment conditions can be obtained with numerical tools such as Finite Elements (FE) and Finite Difference (FD) that produce a discretized version of the distributed partial differential equations (PDEs) that model the heat-transfer [9]. Convective heat transfer problems in heat exchangers can be modelled using Computational Fluid Dynamics solvers (CFD). The discretization process results in very large systems of equations that is computationally very expensive hindering the ability to conduct parametric studies.

In order to reduce the computational complexity caused by the simulation of complex distributed dynamical systems, model order reduction (MOR) techniques have proposed. MOR techniques applied to thermal problems use the discretized version of the underlying PDEs generated using either FE or FD methods to produce a reduced order model which significantly reduce computational complexity, whilst guaranteeing reasonably accurate results [10]-[18]. In order to use MOR techniques in design studies, it is desirable that the reduced order model conserves a dependency on a design parameter, e.g. the coolant mass flow rate, without the need to repeat the reduction process for each variation in parameters. Parametric model order reduction of thermal compact model has been introduced in [10]. The paper presents a parametric MOR method that conserves parameters and demonstrates its application to a case where the boundary conditions representing a forced air cooled heatsink are modelled through several heat transfer coefficient parameters which are kept in the reduced order model. The method, based on multi-moment matching and block Arnoldi's orthogonalization on standard Krylov subspaces, is analytically derived. The method is illustrated and its benefits demonstrated with reference to a power module mounted on a forced air cooled finned heatsink. Detailed comparisons with commercial CFD software and experimental measurements demonstrate the accuracy and computational efficiency of the proposed method.

II. Parametric Model Order Reduction

The establishment of the thermal model of a power module and its cooling assembly requires a mathematical model based on geometry which facilitates the optimization of component

placement, distances, etc. The structure of a typical power module of the type analysed in the paper is shown in Fig 1. The geometry consists of 9 layers including the semiconductor chip, the direct copper bonded (DCB) ceramic substrate a copper ground plane, an aluminium heatsink as well as solder joints between the chips and substrates and thermal interface material between the baseplate and the heatsink.

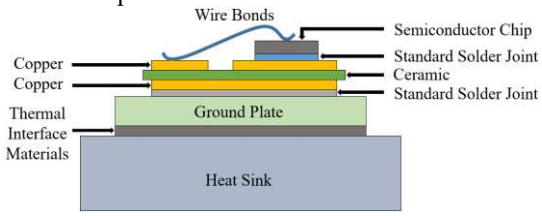

Fig 1. Cut view of a typical power module

It is assumed that every surface of the simplified model are insulated except that the bottom surface is a convection boundary. The temperature distribution $T(x,y,z,t)$ in a solid medium can be obtained by solving the heat conduction PDE:

$$\nabla(K\nabla T) + Q - C\frac{\partial T}{\partial t} = 0 \tag{1}$$

The 3D PDE (1) can be solved numerically by calculating the solution on a discrete mesh. For simplicity, the discretization assumes equal spacing in the horizontal (x,y) plane, while the discretization in the vertical z direction is variable, depending on the relative thickness of each layer. The thermal conductivity $K(x,y,z)$, the heat source $Q(x,y,z,t)$ and the heat capacity $C(x,y,z)$ are function of the position of each point (x,y,z) of the discretization, depending on the material property associated with the point in position (x,y,z). In this way, all different material properties of each layer can be taken into account. The discretization results in a Multi-Input Multi-Output (MIMO) system of ordinary differential equations (ODE) which can be represented in state space form as:

$$\begin{aligned} C\dot{T} + KT &= F \cdot Q(t) \\ y &= E^T \cdot T \end{aligned} \tag{2}$$

$F \in \mathbb{R}^{n\times m}$ and $E \in \mathbb{R}^{n\times p}$ are the input and the output matrix, and m and p denote the number of inputs and outputs, respectively [12-13]. Depending on the complexity of the geometry and the spatial resolution, i.e. the size of the mesh, very large dimension of the ODEs system (2) is required. The full order model results in a system with a matrix-size of $n = 48595$ and the number of inputs is $m = 12$ corresponding to 12 temperature nodes per MOSFET. The self-heating single-chip model can also be extended to multi-chip model using the concepts of cross heating.

A. Conventional Model Order Reduction

MOR is typically achieved by transforming the *n*-dimensional system (2) into a system of lower dimensionality *r* but in the same form [12]:

$$\begin{aligned} C_r\dot{z} + K_r z &= F_r \cdot Q(t) \\ y_r &= E_r^T \cdot z \end{aligned} \tag{3}$$

where $z \in \mathbb{R}^r$. The reduction is obtained by projecting the original state T onto a sub-space of dimension $r \ll n$ with a linear transformation:

$$T = V \cdot z + error \tag{4}$$

The transformation is obtained by a projection process based on the Padé-type approximation where the reduced-order system matrices are obtained as: $C_r = V^T C V$, $K_r = V^T K V$, $F_r = V^T F$, $E_r = V^T E$ [13]. The projection matrix V is an output of an iterative type Arnoldi algorithm projection on a Krylov subspace. The method proposed here, based on [14]-[16], use the idea of moment matching, where moments are defined as the coefficients of the Taylor series expansion of the rational transfer function representing (2) in the frequency domain. Transforming (2) into the frequency domain result in a matrix-valued rational transfer function $G: C \to C^{p\times m}$ given by:

$$G(s) = E^T \cdot (K + sC)^{-1} \cdot F, \qquad s \in \mathbb{C} \tag{5}$$

which can be rewritten as:

$$G(s) = E^T \cdot (I - (-K^{-1}C)s)^{-1} \cdot (K^{-1}F) \tag{6}$$

The block Arnoldi method obtains the information of the leading Taylor coefficients of $G(s)$. Expanding $G(s)$ in (6) around a point s_0:

$$G(s) = \sum_{i=0}^{\infty} E \cdot M_i\, s^i \tag{7}$$

Where the moments M_i are given by:

$$M_i = [(-(s_0C + K))^{-1}C]^i \cdot (s_0C + K)^{-1} \cdot F \tag{8}$$

If, for simplicity, $s_0 = 0$, then $M_i = (-K^{-1}C)^i \cdot (K^{-1}F)$, therefore, matching the moments of the reduced order model to the first i moments of the original system (7) can be obtained by selecting the projection matrix V:

$$V = Kr^i(A,B) = span([B\ AB\ A^2B\ \ldots\ A^{N-1}B]) \tag{9}$$

$Kr^N(A,B)$ is so-called block Krylov subspace, where $A = -K^{-1}C$ and $B = K^{-1}F$. m columns of the matrix $B = [b_1\ b_2\ \ldots\ b_m]$ are starting vectors of the block Krylov subspace $Kr^N(A,B)$. The moment matching based on Krylov subspaces is expressed to find a low-dimensional model that matches the first moments in the Taylor expansion shown in (8). A reduction to a specified order r is obtained by selecting a subspace spanned by an orthogonal basis formed by the first r columns of $K^i(A,B)$. A numerically stable method to generate orthogonal basis vectors of this subspace, based on the Arnoldi process, is detailed in the Appendix 1.

B. Parametric Model Order Reduction

Similarly to the non-parametric case, ODEs system of the form (1) and (2) are considered. In this case, it is assumed that the convection boundary layer has a multi-parameter dependence on air mass flow. The MIMO system with heat transfer coefficients $h_1 h_2 \ldots h_n$ in discretized form is given by:

$$C \cdot \dot{T} + (K + h_1K_1 + h_2K_2 + \cdots + h_nK_n) \cdot T = F \cdot Q(t)$$
$$y = E^T \cdot T \tag{10}$$

Many methods for multi-parametric order reduction have been proposed. There are two main strategies based on the reduction with multi-moment matching, such as [14-20] or reduction without multi-moment matching [21] [22]. In this paper, reduction with multi-moment matching is introduced. The process is based on the Taylor-series expansion of the transfer function $G(s)$ but, this time, in series of the parameters $h_1, \dots, h_n$. The moments of the transfer function are the coefficients of this Taylor series expansion. The derivation will be based on the assumption that the mixing moments can be ignored, as discussed later in this section [23]-[25]. The block Arnoldi's orthogonalization based on standard Krylov subspaces for multi-moment matching needs to be applied [12] [13]. The multi-parameter model will be derived for a 2-parameter case for simplicity, but can be easily extended to any number of parameters. The MIMO system with two parameters h_1 and h_2 in discretized form is given by:

$$C \cdot \dot{T} + (K + h_1K_1 + h_2K_2) \cdot T = F \cdot Q(t)$$
$$y = E \cdot T \tag{11}$$

The Taylor series expansion of the transfer function form of (11) is:

$$\begin{aligned} G(s) &= E \cdot (K + h_1K_1 + h_2K_2 + sC)^{-1} \cdot F \\ &= E[I - (-(K + h_1K_1 + h_2K_2)^{-1}Cs)]^{-1} \\ &\quad \cdot (K + h_1K_1 + h_2K_2)^{-1}F \\ &= E\sum_{i=0}^{\infty}\left[-\begin{pmatrix}K+h_1K_1\\+h_2K_2\end{pmatrix}^{-1}C\right]^j\begin{pmatrix}K+h_1K_1\\+h_2K_2\end{pmatrix}^{-1}Fs^j \\ &= E\sum_{i=0}^{\infty}M_is^i \end{aligned} \tag{12}$$

Where $M_i, i = 0,1, \dots$ are the moments of $G(s)$ in the expansion in series of s. When $i = 0$;

$$\begin{aligned} M_0 &= (K + h_1K_1 + h_2K_2)^{-1}F \\ &= \left(I - \left(-K^{-1}(h_1K_1 + h_2K_2)\right)\right)^{-1}K^{-1}F \end{aligned} \tag{13}$$

When $i = 1$;

$$\begin{aligned} M_1 &= -\begin{pmatrix}K+h_1K_1\\+h_2K_2\end{pmatrix}^{-1}C\begin{pmatrix}K+h_1K_1\\+h_2K_2\end{pmatrix}^{-1}F \\ &= -(K + h_1K_1 + h_2K_2)^{-1}CM_0 \\ &= -\left(I - \left(-K^{-1}(h_1K_1 + h_2K_2)\right)\right)^{-1}K^{-1}CM_0 \end{aligned} \tag{14}$$

For the ith moment,

$$\begin{aligned} M_i &= \left[-\begin{pmatrix}K+h_1K_1\\+h_2K_2\end{pmatrix}^{-1}C\right]^i\begin{pmatrix}K+h_1K_1\\+h_2K_2\end{pmatrix}^{-1}F \\ &= [-(K+h_1K_1 + h_2K_2)^{-1}C]M_{i-1} \\ &\dots \\ &= [-(K+h_1K_1 + h_2K_2)^{-1}C]^iM_0 \\ &= \left[-\left(I - \left(-K^{-1}(h_1K_1 + h_2K_2)\right)\right)^{-1}\right]^i[K^{-1}C]^iM_0 \end{aligned} \tag{15}$$

The term $f(h_1, h_2) = \left(I - \left(-K^{-1}(h_1K_1 + h_2K_2)\right)\right)^{-1}$ appearing in $M_0, M_1, \cdots, M_j$ is an infinitely differentiable function in an open neighborhood around $(h_1, h_2) = (0,0)$, therefore it can be expressed using the multi-variable Taylor expansion as:

$$\begin{aligned} &f(h_1, h_2) = f(0,0) \\ &+\frac{1}{1!}[f_{h_1}(0,0)h_1 + f_{h_2}(0,0)h_2] \\ &+\frac{1}{2!}[f_{h_1h_1}(0,0)h_1^2 + 2f_{h_1h_2}(0,0)h_1h_2 + f_{h_2h_2}(0,0)h_2^2] \\ &+\cdots \\ &= I - K^{-1}(K_1h_1 + K_2h_2) + \left(-K^{-1}(K_1h_1 + K_2h_2)\right)^2 + \cdots \\ &= \sum_{i_0=0}^{\infty}(-K^{-1}(K_1h_1 + K_2h_2))^{i_0} \end{aligned} \tag{16}$$

Consequently, M_0 in (13) can be written as (17)

$$M_0 = \sum_{i_0=0}^{\infty}(-K^{-1}(K_1h_1 + K_2h_2))^{i_0}K^{-1}F \tag{17}$$

As mentioned before, a simplification can be achieved if mixing moments can be ignored. This is based on the assumption that $K_1 \cdot K_2 = 0$. For the problem under investigation, i.e. the thermal analysis of power modules with convective boundary conditions, the parameters series $h_1\ h_2 \dots h_n$ and submatrices $K_1\ K_2 \dots K_n$ only appear in the equations of the states on boundary layer of the baseplate.

The temperature distribution $T(x, y, z)$ is discretized and stored in a square system of dimension of $n = n_xn_yn_z$. x- and y-axis represent the temperature probes on horizontal layers while z-axis represents the vertical temperature distributions. Thermal capacity and conductivity matrices $C, K, K_1, K_2 \dots$ are sparse matrices with only few non-zero elements. According to the heat transfer equation, the non-zero elements of K, K_1 and K_2 are the inverse value of the heat thermal resistances between nodes of the discretization. Fig 2 visually illustrates the heat conduction matrix on the n_zth layer.

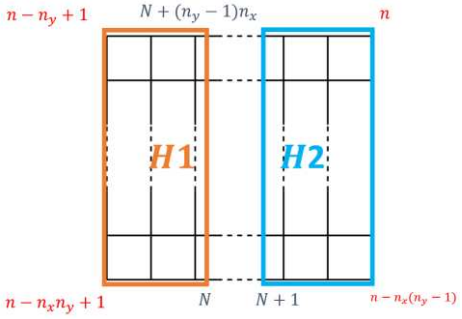

Fig 2. 2-D diagram for analysis of heat transfer matrix on the n_z th layer

The 2-D illustration shows that the heat transfer matrix is divided into two sections. The non-zero elements of K_1 are contained in the left (orange) area with heat transfer coefficient h_1 and are zero elsewhere and vice versa for K_2. For example, for the nth node, the heat transfer is non zero only between its adjacent nodes, which are $(n-1)$ th, $(n-n_x)$ th and $(n-n_x n_y)$th. This means that the non-zero elements of the nth row are only located in the nth, $(n-1)$th, $(n-n_x)$th and $(n-n_x n_y)$ th columns. Consequently, matrix K_1 and K_2 can be expresses as shown in (18).

$$K = \begin{bmatrix} E_{conduction} \\ E_{zeroK} \end{bmatrix}$$

$$K_1 = \begin{bmatrix} E_{zeroK_1} \\ E_{h_1} \end{bmatrix}$$

$$E_{h_1} = \begin{bmatrix} \ddots & \vdots & \vdots & \vdots & \vdots \\ \cdots & E_{(n-n_x n_y+1,\ n-n_x n_y+1)} & E_{(n-n_x n_y+1,\ n-n_x n_y+2)} & \cdots & 0 \\ \cdots & E_{(n-n_x n_y+2,\ n-n_x n_y+1)} & E_{(n-n_x n_y+2,\ n-n_x n_y+2)} & \cdots & 0 \\ \cdots & \vdots & \vdots & \ddots & 0 \\ \cdots & 0 & 0 & 0 & 0 \end{bmatrix}$$

$$K_2 = \begin{bmatrix} E_{zeroK_2} \\ E_{h_2} \end{bmatrix}$$

$$E_{h_2} = \begin{bmatrix} \ddots & \vdots & \vdots & \vdots & \vdots \\ \cdots & 0 & 0 & 0 & 0 \\ \cdots & 0 & \ddots & \vdots & \vdots \\ \cdots & 0 & \cdots & E_{(n-1,\ n-1)} & E_{(n-1,\ n)} \\ \cdots & 0 & \cdots & E_{(n,\ n-1)} & E_{(n,\ n)} \end{bmatrix} \quad (18)$$

In (18), $K\ K_1\ K_2 \in \mathbb{R}^{n\times n}$, while $E_{conduction}\ E_{zeroK_1}\ E_{zeroK_1} \in \mathbb{R}^{(n-n_x n_y)\times n}$ and $E_{zeroK}\ E_{h_1}\ E_{h_2} \in \mathbb{R}^{(n_x n_y)\times n}$. It is evident that the locations of non-zero elements in K_1 and K_2, results in $K_1 \cdot K_2 = 0$. Similar assumption and derivation can be applied in the case with more than 2 parameters. The terms containing the parameters in (17) can be further simplified using:

$$(h_1K_1 + h_2K_2)^{\,i_0} \approx (K_1 + K_2)^{\,i_0}\frac{{h_1}^{i_0} + {h_2}^{i_0}}{2} \quad i_0 = 0,1,\dots\infty$$

The error in this approximation can be expressed as:

$$K_e = (h_1K_1 + h_2K_2)^{\,i_0} - (K_1 + K_2)^{\,i_0}\frac{{h_1}^{i_0} + {h_2}^{i_0}}{2}$$

$$= \frac{{h_1}^{i_0} - {h_2}^{i_0}}{2}({K_1}^{i_0} - {K_2}^{i_0}) \quad (19)$$

Where

$$K_e(\,i_0 = 0) = 0$$

$$K_e(\,i_0 = 1) = \frac{h_1 - h_2}{2}(K_1^1 - K_2^1)$$

$$\dots \quad (20)$$

$$K_e(\,i_0 = i_\infty) = \frac{(h_1 - h_2)\begin{pmatrix} {h_1}^{i_\infty-1} + {h_1}^{i_\infty-2}h_2 \\ +\cdots \\ h_1{h_2}^{i_\infty-2} + {h_2}^{i_\infty-1} \end{pmatrix}}{2}\left({K_1}^{i_\infty} - {K_2}^{i_\infty}\right)$$

It can then be concluded that the smaller $h_1 - h_2$, the smaller the error. This can be achieved with a finer discretization of the convective heat transfer at the boundary condition: assuming there are n heat transfer coefficients $h_1 h_2$ ... h_n, the error will be proportional to $(h_1 - h_2)(h_2 - h_3)$ ... $(h_{n-1} - h_n)$. With an increasing n, the step difference of adjacent parameters $h_{n-1} - h_n$ will reach zero, and error K_e approaches zero correspondingly. Based on the above two assumptions, the term (17) can be rewritten as:

When $i = 0$;

$$M_0 = \sum_{i_0}^{\infty}\left(-K^{-1}(K_1+K_2)\right)^{i_0}K^{-1}F({h_1}^{i_0} + {h_2}^{i_0})/2 \quad (21)$$

When $i = 1$;

$$M_1 = -\left(I - \left(-K^{-1}(h_1K_1 + h_2K_2)\right)\right)^{-1}K^{-1}CM_0$$

$$= \left[-\sum_{i_1}^{\infty}\left(-K^{-1}(K_1 + K_2)\right)^{i_1}K^{-1}C({h_1}^{i_1} + {h_2}^{i_1})/2\right]$$

$$\cdot\left[\sum_{i_0}^{\infty}\left(-K^{-1}(K_1+K_2)\right)^{i_0}K^{-1}F({h_1}^{i_0} + {h_2}^{i_0})/2\right] \quad (22)$$

For the ith moment,

$$M_i = [-(K+h_1K_1 + h_2K_2)^{-1}C]M_{i-1}$$

$$= \left[-\sum_{t_i}^{\infty}\left(\left(-K^{-1}(K_1+K_2)\right)^{t_i}K^{-1}C({h_1}^{t_i} + {h_2}^{t_i})/2\right)\right]\cdot M_{i-1}$$

$$= \left[-\sum_{t_i}^{\infty}\left(\left(-K^{-1}(K_1+K_2)\right)^{t_i}K^{-1}C({h_1}^{t_i} + {h_2}^{t_i})/2\right)\right]$$

$$\cdot\left[-\sum_{t_{i-1}}^{\infty}\left(\left(-K^{-1}(K_1+K_2)\right)^{t_{i-1}}K^{-1}C({h_1}^{t_{i-1}} + {h_2}^{t_{i-1}})/2\right)\right]\cdot M_{i-2}$$

$$= (-1)^i\sum_{t_i=0}^{\infty}\sum_{t_{i-1}=0}^{\infty}\dots\sum_{t_1=0}^{\infty}\sum_{t_0=0}^{\infty}\begin{bmatrix} \left(-K^{-1}(K_1+K_2)\right)^{t_i}K^{-1}C \\ \cdot\left(-K^{-1}(K_1+K_2)\right)^{t_{i-1}}K^{-1}C \\ \dots \\ \cdot\left(-K^{-1}(K_1+K_2)\right)^{t_1}K^{-1}C \\ \cdot\left(-K^{-1}(K_1+K_2)\right)^{t_0}K^{-1}F \end{bmatrix}$$

$$\cdot\left(\frac{{h_1}^{t_i} + {h_2}^{t_i}}{2}\right)\left(\frac{{h_1}^{t_{i-1}} + {h_2}^{t_{i-1}}}{2}\right)\dots\cdot\left(\frac{{h_1}^{t_1} + {h_2}^{t_1}}{2}\right)\left(\frac{{h_1}^{t_0} + {h_2}^{t_0}}{2}\right) \quad (23)$$

As demonstrated in (21)-(23), the parameters h_1 and h_2 are separated from the system matrices. Consequently, it is possible to make the subspace $span(M_0, M_1, M_2, \dots M_i)$ independent of the parameters. The first moment M_0 can then be expressed as the Krylov subspace:

$$spancol\{V_0\} = Kr^{i_0}(-K^{-1}(K_1 + K_2), K^{-1}F) \quad (24)$$

Similar methods can be applied in the multi-parameter system with more than two parameters in (10) as (25).

$$spancol\{V_0\} = Kr^{i_0}(-K^{-1}(K_1 + K_2 + \cdots + K_n), K^{-1}F) \quad (25)$$

The generation of orthogonal basis vectors of this subspace, based on the Arnoldi process, is reported in the Appendix II. The proposed MOR procedure can be summarized in the following steps:

1. The heat transfer eq. (1) is discretized using Finite Difference (or FE) methods into a set of parametric ODE of order N (10) dependent on the parameters $h_{1,\dots}h_n$
2. The first k moments $M_k, i = 0, \dots, k$ of the Taylor series of the transfer function are calculated using (21)-(23) which are, by definition, Krylov subspaces as in (24)
3. The Arnoldi method (Appendix) is applied to generate a numerically stable, orthogonal basis sets for the Krylov subspaces, resulting in the projection matrix V of dimension $r \ll N$
4. The original system (2) of order N is now reduced to (3) of order r, where the dependence on the parameters is conserved in the system matrices C_r, K_r, F_r

III. Thermal Modelling of Air Cooling System

Given the difficulty of modelling a complex cooling system such as a parallel plate heatsink with variable flow rates, it is common to replace the cooling system with an equivalent convective boundary condition. This can be either a single constant heat transfer coefficient, or a variable heat transfer coefficient changing along the axis, if the length and/or pressure drop along the heatsink is significant. An analytical model, based on [26] and [27], is presented here to derive an equivalent convective boundary condition for modeling a parallel plate heatsink. With reference to a standard parallel plate heatsink where s and t are the fin spacing and fin thickness of heat sink respectively, c is fin height, b is heat sink width and n is the number of heat sink channels, the heat transfer h can be expressed as:

$$h(z^*) = \frac{Nu_{\sqrt{A}}(z^*) \times \lambda_{air}}{d_h}$$
$$\text{with } d_h = \frac{2sc}{s+c} \text{ and } s = \frac{b-(n+1)t}{n} \quad (26)$$

Where the dimensionless thermal duct length or axial position is given by:

$$z^* = \frac{\mu z}{\dot{m} P_r} \quad (27)$$

μ is the dynamic viscosity of air, z is the axial position in the heatsink channel, $\dot{m}$ is mass flow rate of air, λ_{air} is thermal conductivity of air, and P_r is Prandtl number of air with an approximated value of 0.71. Based on the transfer between actual and dimensionless thermal duct length, an analytical model for the local Nusselt number ($Nu_{\sqrt{A}}$) with different axial position can be established [27] for the heat sink model, as follows:

$$N_{u\sqrt{A}}(z^*) = [\left(\frac{C_4 f(Pr)}{\sqrt{z^*}}\right)^m + (\{\{C_1(\frac{fRe_{\sqrt{A}}}{8\sqrt{\pi}\epsilon^\gamma})\}^5 + \{C_2 C_3(\frac{fRe_{\sqrt{A}}}{z^*})^{\frac{1}{3}}\}^5\right]^{\frac{m}{5}}]^{\frac{1}{m}} \quad (28)$$

Where m is the model blending parameter and other parameters of (28) are provided in [28].
The analytical model is solved for UWF (uniform wall flux) and UWT (uniform wall temperature) boundary conditions [26]. The heat sink material is aluminium and due to the high thermal conductivity, the presented investigation assumes UWT. For UWT boundary conditions, the function $f(Pr)$ is provided by

$$f(Pr) = \frac{0.564}{\left[1 + \left(1.664 P_r^{\frac{1}{6}}\right)^{\frac{9}{2}}\right]^{\frac{2}{9}}} \quad (29)$$

The friction factor-Reynolds number product in (28) is given by

$$f\,Re_{\sqrt{A}} = \frac{12}{\sqrt{\epsilon}(1+\epsilon)\left[1 - \frac{192\epsilon}{\pi^5}\tanh\left(\frac{\pi}{2\epsilon}\right)\right]} \quad (30)$$

where ϵ is heat sink channel aspect ratio and

$$\epsilon = \frac{\text{fin thickness}}{\text{channel space}} \quad (31)$$

IV. Thermal Model Experiment and Simulation Results

Experimental validation of the proposed MOR technique is presented in this section with reference to a configuration, with one power module and two power resistors acting as heat sources. Both the two resistors and power module are mounted on the heatsink via thermal pad (Kerafol KERATHERM Thermal Pad 6.5W/mK Gap Fill) to ensure good heat transfer.

A. Power Module

The power module used in this work is a Silicon Carbide (SiC) MOSFET-based half-bridge. Based on innovative wire-bond free planar interconnect technology [29]-[30], the module has been designed and manufactured by Siemens AG, within the Horizon2020 European Project - Integrated, Intelligent Modular Power Electronic Converter (I2MPECT) [31], to provide a power electronic building block (PEBB) for a 99% efficient 3-phase power converter with a power-to-weight ratio of 10 kW/kg. This means that for output power of 45 kW, maximum three-phase power loss of 450 W (150 W per phase/leg) is the allowable limit. Fig 3 shows CAD drawings of the half-bridge wire-bondless power module. Twelve MOSFETs are pressure silver sintered onto the substrate copper base plate. The power module contains 12 SiC MOSFETs (CPM2-1200-0025B). The module substrate is a DCB (direct copper bonding) substrate. The module is primary cooled via the baseplate, which is designed to be mounted to an air cooled heatsink via a thermal interface material.

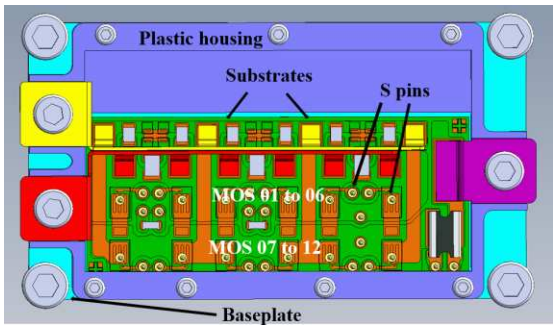

Fig 3. CAD drawings of single I2MPECT power module

B. Force-Air Cooling System

The heatsink used in these experiments is a typical hollow-fin heatsink (Fischerelectronik) with an integrated axial fan, as shown in Fig 4.

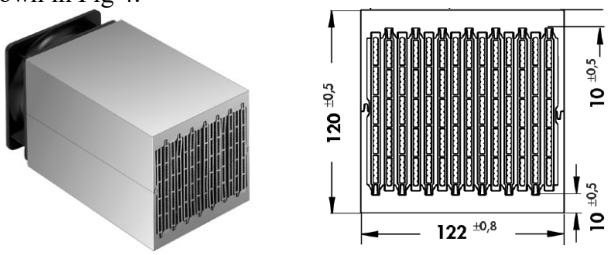

(a) (b)

Fig 4. Hollow-fin cooling aggregates. (a) The prototype of heatsink; (b) Cross-section layout of heatsink

The outlet air temperature of heat sink needs be limited in 55-65 ℃ with an inlet air temperature of 40 ℃. The fluid heat transfer equation is expressed in (32)

$$\Delta Q = cm\Delta T \quad (32)$$

Where ΔQ is the heat flowing into the heat sink to increase the air temperature by ΔT while c and m are the specific heat and mass flow rate of air. With a maximum three-phase power loss of 450 W, inlet air flow with an approximate range of 1m/s to 2m/s is suitable for the system cooling. Applying the analytical model in (26)-(28), the resulting heat transfer coefficient as function of the axial distance from the inlet for the heatsink is shown in Fig 5 for three different values of air mass flow from 1m/s to 2m/s. The analytical model has been validated against detailed simulation using CFD software Ansys Icepak as shown in Fig. 6.

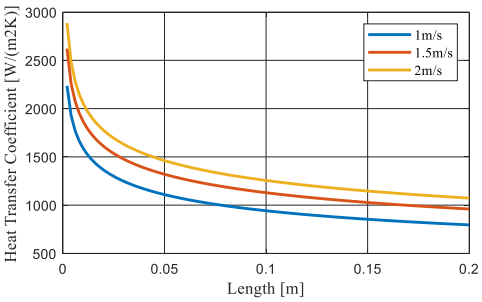

Fig 5. Heat transfer coefficient along the axial direction of the air flow

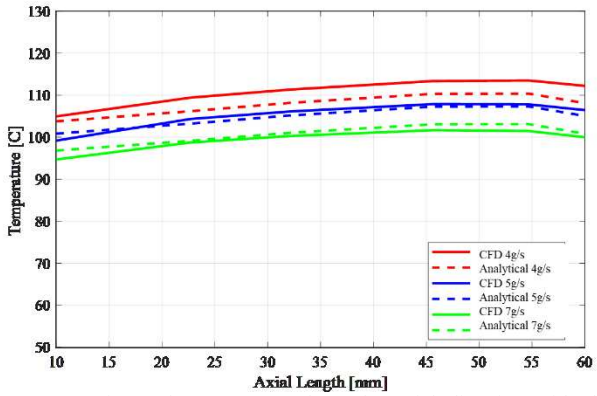

Fig 6. Comparison of temperature along the axial direction with the analytical model and detailed CFD analysis

D. Experimental Setup and Simulation Results

Fig 7 shows the experimental setup used to evaluate the proposed models. There are four thermocouples installed, positioned in the airflow at the inlet, outlet and in between the modules, allowing the air temperature to be monitored. Additionally, a Fibre optic temperature measurement probe is positioned in direct contact with one of the MOSFET die to measure its temperature directly and provide a reference for comparison with the analytical model predictions.

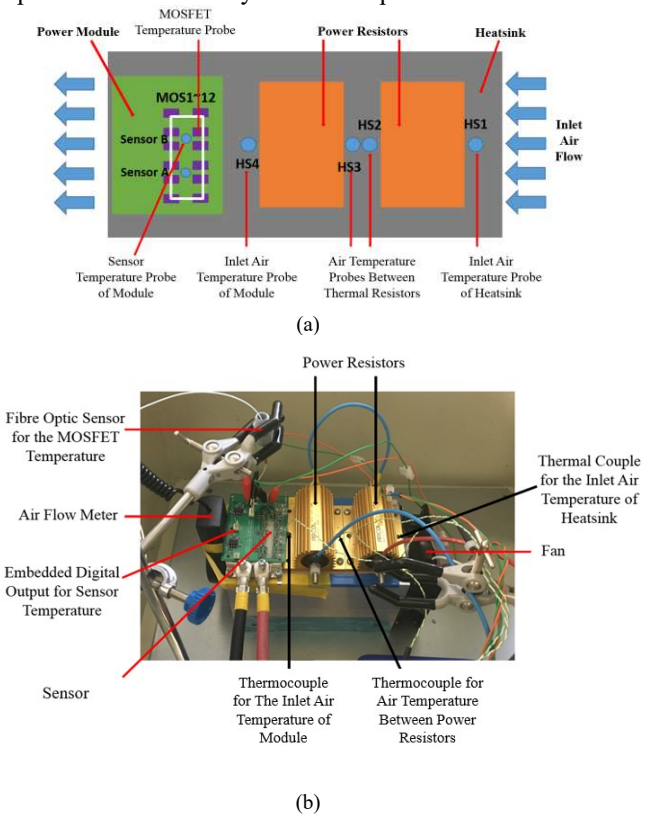

Fig 7. Experimental layout. (a) Thermal model design; (b) General view of experimental components.

The influence of convective boundary condition in experiment is shown in Fig 8. The convective boundary condition is affected by the air flow rate. Based on the same input power and experiment layout, the steady state temperature

captured by thermal camera can shows the effect of the change of the air flow rate on convective boundary condition. With an increasing air flow rate from 1m/s to 1.5m/s, the maximum temperature of the power module in steady state reduces from 98℃ to 82℃.

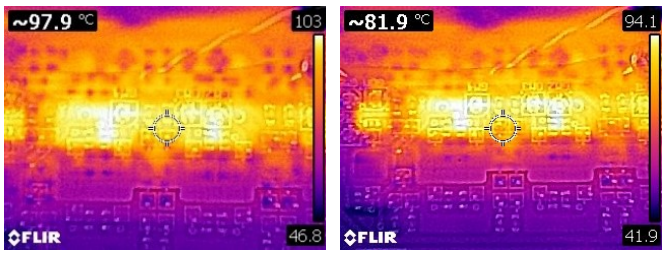

(a) (b)

Fig 8. Steady-State temperature from thermal camera. (a)1m/s for peak current of 70A; (b)1.5m/s for peak current of 70A;

The proposed MOR method is applied to the system. Fig 9 illustrates surface temperature responses of the 11-th MOSFET in Fig 3 calculated by MOR and compared to transient results obtained with experiment and commercial FE software ANSYS. As can be seen in Fig. 10, the agreement between the proposed reduced order methods and experiment is good, especially in steady state conditions, while in transient condition an error of less than 10% is noted.

The discretization employed in the full order model results in a system with 48595 nodes, while the reduced order has 12 states corresponding to 12 temperature nodes per MOSFET. On the same computer and with the same mesh size, ANSYS takes over 500 minutes while the reduced-order simulation only takes about 5 seconds.

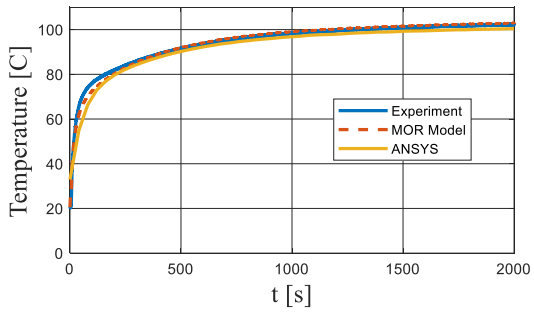

(a)

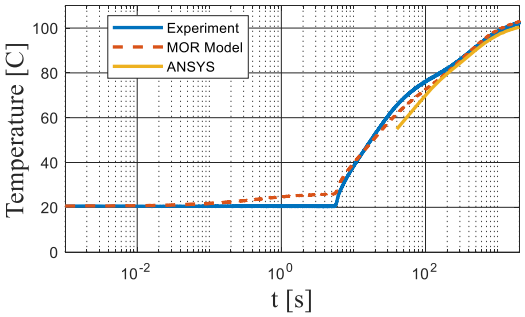

(b)

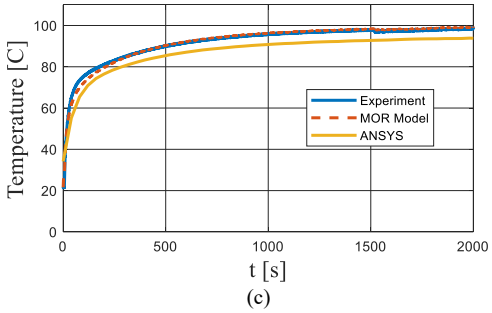

(c)

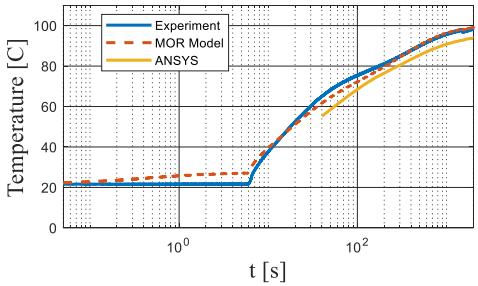

(d)

Fig 9. Comparison between experimental data and estimated values. (a)1m/s for peak current of 90A; (b)Log plot of (a); (c)1.5m/s for peak current of 90A; (d) Log plot of (c).

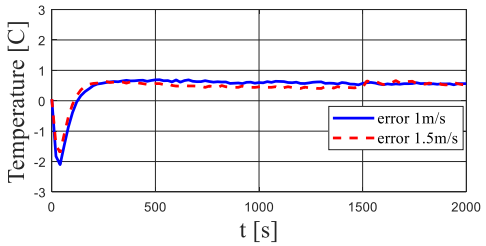

Fig 10. Transient error of MOR compared with experiment.

In Fig 11, a more complex boundary condition is introduced to test the accuracy of the parametric MOR analytical model. In this test the air-flow velocity and the DC current are variable following the profiles shown in Fig 11(a). A good accuracy is demonstrated for the reduced order model.

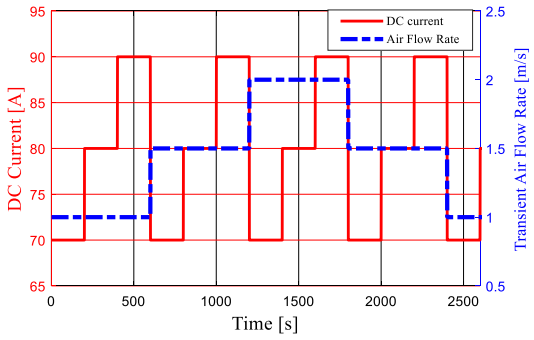

(a)

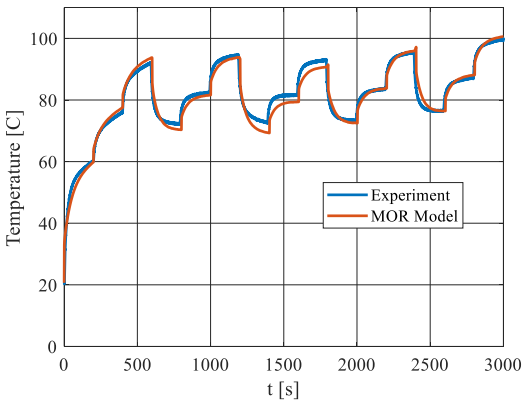

(b)

Fig 11. Comparison between experimental data and estimated values with time-varied DC current and transient air flow rate. (a) Module current and transient air flow rate; (b) Transient thermal response from experiment and MOR model.

V. Conclusion

In this paper, a novel multi-parameter order reduction is developed and applied to a power module with forced-air-cooling systems. The multi-moment matching technique is used to preserve in the reduced order a number of parameters, making calculations in variable operating conditions significantly more efficient. An example of a power module cooling system with different mass air flow rates is reported and experimental data proves the accuracy of this reduced-order analytical model. A significant increase in computational efficiency is demonstrated resulting in faster calculation time and memory requirements. The method can have applications at both the design stage and during operation of power conversion systems. Optimization of layout in power electronics modules and converters design might require many iterations using different values of parameters e.g. of materials or cooling conditions. With the proposed parametric MOR such applications can be greatly simplified as the reduced order model conserves dependency on parameters which can be simply modified at each iteration without requiring additional computations. Thanks to its low computational complexity, the resulting reduced order model can also be used in real-time applications as an observer for temperature estimation of power devices during converter operation.

APPENDIX. I
ARNOLDI'S ORTHOGONALIZATION

Algorism	Description
$v_i = B_i/\|B_i\|$	Start computation of v_{i+1}
$for\ j = 1, \dots, j_{max} - 1$	One matrix multiplication
$t = Av_i$	t is in the space K_{j+1}
$h_{ij} = v_i^T t$	$h_{ij} v_i$= projection of t on v_i
$t = t - h_{ij} v_i$	Subtract that projection
end	t is orthogonal to $v_1, \dots, v_j$
$h_{j+1,j} = \|t\|$	Compute the length of t
$v_{j+1} = t/h_{j+1,j}$	Normalize t to $\|v_{j+1}\|$=1
end	$v_1, \dots, v_{jmax}$ are orthonormal

References

[1] H. Wang, M. Liserre, and F. Blaabjerg, "Toward reliable power electronics: Challenges, design tools, and opportunities," *IEEE Ind. Electron. Mag*., vol. 7, no. 2, pp. 17–26, 2013.

[2] S. Yang, A. Bryant, P. Mawby, D. Xiang, L. Ran, and P. Tavner, "An industry-based survey of reliability in power electronic converters," *IEEE Trans. Ind. Appl*., vol. 47, no. 3, pp. 1441–1451, 2011.

[3] T. Herrmann, M. Feller, J. Lutz, R. Bayerer, and T. Licht, "Power cycling induced failure mechanisms in solder layers," in *Proc. 2007* Eur. *Conf. Power Electron. Appl.,* Sep. 2007, pp. 1–7.

[4] M. Gerber, J. A. Ferreira, N. Seliger, and I. W. Hofsajer, "Integral 3-D thermal, electrical and mechanical design of an automotive DC/DC converter," *IEEE Trans. Power Electron*., vol. 20, no. 3, pp. 566–575, May 2005.

[5] Smet, V., Forest, F., Huselstein, J.-J., et al.: "Ageing and failure modes of IGBT modules in high-temperature power cycling," *IEEE Trans. Ind. Electron*., 2011, 58, (10), pp. 4931–4941.

[6] M. Andresen, K. Ma, G. Buticchi, J. Falck, F. Blaabjerg, and M. Liserre, "Junction Temperature Control for More Reliable Power Electronics," *IEEE Trans. Power Electron*., vol. 33, no. 1, pp. 765–776, 2018.

[7] A. Griffo, J. Wang, K. Colombage, T. Kamel, "Real-Time measurement of temperature sensitive electrical parameters in SiC power MOSFETs," *IEEE Trans. Ind. Electron.*, vol. 65, no. 3, pp. 2663–2671, March 2018

[8] M. Iachello, V. De Luca, G. Petrone, N. Testa, L. Fortuna, G. Cammarata, S. Graziani, M. Frasca, "Lumped parameter modelling for thermal characterization of high-power modules", IEEE Trans. Comp. Packaging and Manuf. Tech., vol. 4, n.10, pp. 1613-1623, Oct. 2014.

[9] G. D. Smith, *Numerical solution of partial differential equations: finite difference methods*. Oxford, U.K.: Oxford Univ. Press, 1965.

[10] X. Dong, A. Griffo and J. Wang, "Fast Simulation of transient temperature distributions in power modules using multi-parameter model reduction," *The Journal of Engineering,* vol. 2019, no. 17, pp. 3603-3608, 2019.

[11] M. A. Bazaz, Mashuq-un-Nabi, and S. Janardhanan, "A review of parametric model order reduction techniques," *IEEE International Conference on Signal Processing, Control and Computation*, 2012.

[12] T. Bechtold, E.B. Rudnyi, J. Korvink, "Model order reduction for MEMS: methodology and computational environment for electro-thermal models," *MODEL Order Reduction: Theory, Research Aspects and Applications*, 13(3):403–419, 2008.

[13] R. W. Freund, "Krylov-subspace methods for reduced-order modeling in circuit simulation," *J. Comput. Appl. Math*., vol. 123, no. 1–2, pp. 395–421, 2000.

[14] Y. Li, Z. Bai, Y. Su, and X. Zeng, "Parameterized model order reduction via a two-directional Arnoldi process," in *Proc. Intl. Conf. ComputerAided Design*. San Jose, CA, Nov 2007, pp. 868–873.

[15] Y. T. Li, Z. Bai, Y. Su, and X. Zeng, "Model order reduction of parameterized interconnect networks via a two-directional arnoldi process," *IEEE Trans. Comput. Des. Integr. Circuits Syst*., vol. 27, no. 9, pp. 1571–1582, 2008.

[16] Y. Li, Z. Bai, and Y. Su, "A two-directional Arnoldi process and its application to parametric model order reduction," *J. Comput. Appl. Math*., vol. 226, no. 1, pp. 10–21, 2009.

[17] L. H. Feng, E. B. Rudnyi, and J. G. Korvink, "Preserving the film coefficient as a parameter in the compact thermal model for fast electrothermal simulation," *IEEE Trans. Comput. Des. Integr. Circuits Syst*., vol. 24, no. 12, pp. 1838–1847, 2005.

[18] O. Farle, V. Hill, P. Ingelström, and R. Dyczij-Edlinger, "Multi-parameter polynomial order reduction of linear finite element models," *Math. Comput. Model. Dyn. Syst*., vol. 14, no. 5, pp. 421–434, 2008.

[19] L. Codecasa, "A Novel Approach for Generating Boundary Condition Independent Compact Dynamic Thermal Networks of Packages," *IEEE Transactions on Components and Packaging Technologies*, vol. 28, no. 4, pp. 593–604, 2005.

[20] T. Bechtold, E. B. Rudnyi, and D. Hohlfeld, "System-level model of electrothermal microsystem with temperature control circuit," *2011 12th Int. Conf. Therm. Mech. Multi-Physics Simul. Exp. Microelectron*. Microsystems, EuroSimE 2011, no. March 2015, 2011.

[21] P. K. Gunupudi, R. Khazaka, M. S. Nakhla, T. Smy, and D. Celo, "Passive parameterized time-domain macromodels for high-speed transmission-

line networks," *IEEE Trans. Microw. Theory Tech*., vol. 51, no. 12, pp. 2347–2354, 2003
[22] P. Gunupudi and M. Nakhla, "Multi-dimensional model reduction of VLSI interconnects," Proc. *IEEE 2000 Cust. Integr. Circuits Conf*. (Cat. No.00CH37044), no. 613, pp. 1–4, 2000.
[23] T. Bechtold, D. Hohlfeld, E. B. Rudnyi, and J. G. Korvink, "Moment-matching-based linear model order reduction for nonparametric and parametric electrothermal mems models," *Syst. Model. MEMS*, vol. 10, no. July 2015, pp. 211–235, 2013.
[24] D. Celo, P. K. Gunupudi, R. Khazaka, D. J. Walkey, S. Member, T. Smy, and M. S. Nakhla, "Fast simulation of steady-state temperature distributions in electronic components using multidimensional model reduction," *IEEE Trans. Compon. Packag. Technol*., vol. 28, no. 1, pp. 70–79, 2005.
[25] T. Bechtold, D. Hohlfeld, E. B. Rudnyi, H. Zappe, and J. G. Korvink, "Inverse thermal problem via model order reduction : Determining material properties of a microhotplate," *Proc. 11th International Workshop on Thermal Investigations of ICs and Systems (THERMINIC)*, pp. 28–30, 2005.
[26] Y. S. Muzychka and M. M. Yovanovich, "Laminar forced convection heat transfer in the combined entry region of non-circular ducts," *ASME Trans*., vol. 126, no. 1, pp. 54–61, Feb. 2004
[27] Y. S. Muzychka, "Generalized Models for Laminar Developing Flows in Heat Sinks and Heat Exchangers," *Heat Transf. Eng*., vol. 34, no. 2–3, pp. 178–191, 2013.
[28] Y. S. Muzychka and M. M. Yovanovich, "Pressure drop in laminar developing flow in noncircular ducts: A scaling and modeling approach," *J. Fluids Eng*., vol. 131, no. 11, p. 111105, 2009.
[29] M. Guacci, D. Bortis, I.F. Kovacevic-Badstuner, U. Grossner, J.W. Kolar, "Analysis and Design of a 1200 V All-SiC Planar Interconnection Power Module for Next Generation More Electrical Aircraft Power Electronic Building Blocks", *CPSS Trans. On Power Electronics and Appl.* Vol. 2, n.4, pp. 320-330, Dec. 2017
[30] K. Weidner, M. Kaspar, and N. Seliger, "Planar interconnect technology for power module system integration," in *Proc. of the 7th International Conference on Integrated Power Electronic Systems (CIPS)*, Nuremberg, Germany, 2012.
[31] www.i2mpect.eu

Xiaojun Dong received the B.Eng. degree in hydraulics and hydropower engineering from Northwest A&G University, Yangling, China, in 2014, and the M.Sc. degree in electronics and electrical engineering from University of Sheffield, Sheffield, U.K., in 2015. He is currently working toward the Ph.D. degree in electronics and electrical engineering at The University of Sheffield.
His current research focuses on thermal analysis of power electronics system.

Antonio Griffo (M'12) received the M.Sc. degree in electronic engineering and the Ph.D. degree in electrical engineering from the University of Napoli "Federico II," Naples, Italy, in 2003 and 2007, respectively. From 2007 to 2013, he was a Research Associate with The University of Sheffield, Sheffield, U.K., and the University of Bristol, Bristol, U.K. He is currently a Senior Lecturer in the Department of Electronic and Electrical Engineering, The University of Sheffield. His research interests include modeling, control, and condition monitoring of electric power systems, power electronics converters, and electrical motor drives for renewable energy, automotive, and aerospace applications..

Jiabin Wang (SM'03) received the B.Eng. and M.Eng. degrees from Jiangsu University, Zhenjiang, China, in 1982 and 1986, respectively, and the Ph.D. degree from the University of East London, London, U.K., in 1996, all in electrical and electronic engineering. He is currently a Professor of electrical engineering at The University of Sheffield, Sheffield, U.K. From 1986 to 1991, he was with the Department of Electrical Engineering, Jiangsu University, where he was appointed a Lecturer in 1987 and an Associate Professor in 1990. He was a Postdoctoral Research Associate at The University of Sheffield from 1996 to 1997 and a Senior Lecturer at the University of East London from 1998 to 2001. His research interests range from motion control and electromechanical energy conversion to electric drives for applications in automotive, renewable energy, household appliances, and aerospace sectors.
Dr. Wang is a Fellow of the Institution of Engineering and Technology, U.K